RSC Advances

ROYAL SOCIETY OF CHEMISTRY

www.rsc.org/advances

Graphical Abstract

Multifunctional, Robust, Light Weight, Free Standing MWCNT/Phenolic Composite Paper

as Anode for Lithium Ion Batteries and EMI Shielding Material

Satish Teotia[1], Bhanu Pratap Singh[1*], Indu Elizabeth[1], Vidya Nand Singh[2], R. Ravikumar[3],

Avanish Pratap Singh[4], S. Gopukumar[3], S.K.Dhawan[4], R.B.Mathur[1]

CSIR−Network Institutes for Solar Energy

Multifunctional, robust, light weight, free standing MWCNT/polymer composite of 140 μm thickness is demonstrated as an anode material for li-ion battery and efficient EMI shielding material.
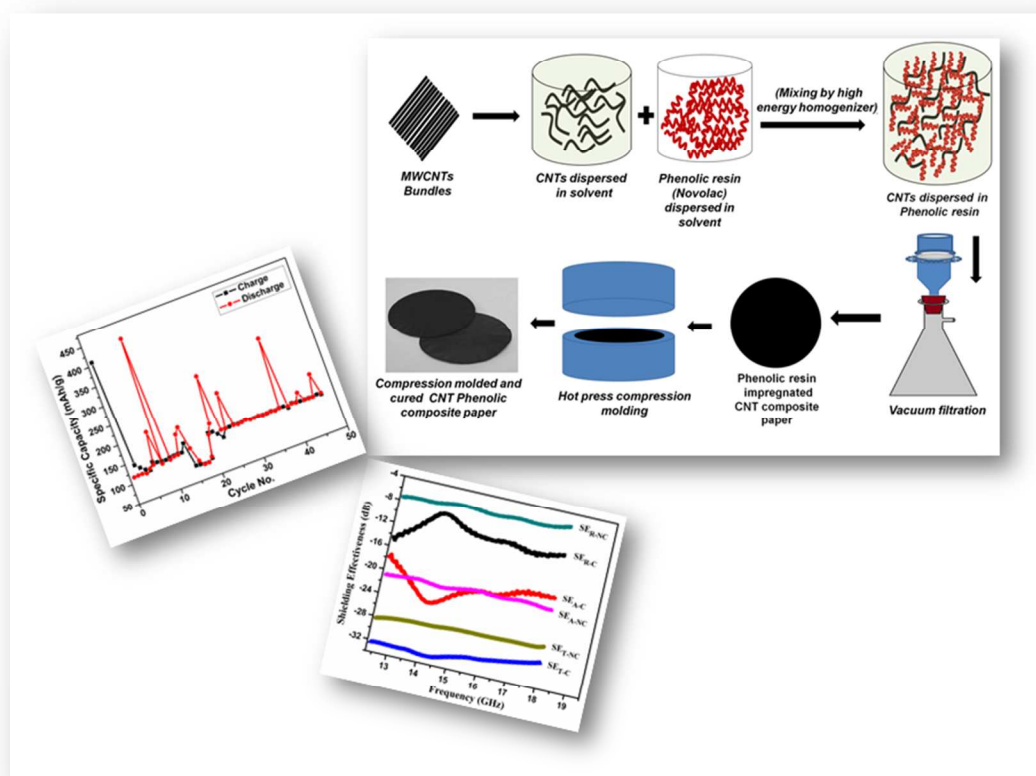
Multifunctional, Robust, Light Weight, Free Standing MWCNT/ Phenolic Composite Paper as Anode for Lithium Ion Batteries and EMI Shielding Material

Satish Teotia[1], Bhanu Pratap Singh[1*], Indu Elizabeth[1], Vidya Nand Singh[2], Raman Ravikumar[3], Avanish Pratap Singh[4], S. Gopukumar[3], S.K.Dhawan[4], Anchal Srivastava[5], R.B.Mathur[1]

CSIR–Network Institutes for Solar Energy

[1]Physics and Engineering of Carbon, CSIR-National Physical Laboratory, New Delhi, India-110012

[2]Electron and Ion Microscopy Section, CSIR-National Physical Laboratory, New Delhi, India-110012

[3]CSIR-Central Electro Chemical Research Institute, Karaikudi, Chennai-630 006

[4]Polymeric and Soft Materials Section, CSIR-National Physical Laboratory, New Delhi, India-110012

[5] Department of Physics, Banaras Hindu University, Varanasi-221005, U.P., India

Abstract

Energy density of Li-ion batteries is marred due to additional weight of copper used as current collector. In this work, fabrication of a strong graphitized multiwalled carbon nanotubes (G-CNTs)/phenolic composite paper using a new dispersion technique is reported. The composite paper has been used as a free standing current collector as well as anode material for Li-ion batteries because of having electrical conductivities in the range of 76 Scm^{-1}. This thin highly conducting composite paper (thickness 140 μm) also shows efficient electromagnetic interference (EMI) shielding of 32.4 dB in Ku-band (12.4-18 GHz waveguides). Structural and morphological studies were carried out using, TEM, and SEM. The flexural strength of the composite paper was 30 MPa which is good enough for use as an electrode in batteries. The electrochemical properties of the composite paper were investigated by galvanostatic charge–

discharge test. It exhibits a stable reversible specific capacity for more that 45 cycles. EMI shielding effectiveness (SE) was measured using a vector network analyzer and the total EMI-SE surpasses the value needed for commercial applications.

Corresponding author; Tel.: +91-11-45608460, Fax: +91-11-45609310
E-mail address: bps@mail.nplindia.ernet.in(BPS)

Introduction

For portable electronics, aeroplanes and vehicles batteries are required. Rechargeable batteries are the best as these are cheaper and produce high power than other storage materials. Li-ion batteries (LIBs) are the most promising rechargeable batteries but the long run performance of LIBs needs to improve. LIBs typically consist of an anode (-ve electrode), a cathode (+ve electrode) and a conducting electrolyte. It stores electrical energy in the two electrodes in the form of Li-intercalation compounds. On charging the LIBs, cathode releases lithium ions which move through electrolyte and get inserted into other electrode. While discharging, the above process is reversed. Thus, Li ions move from anode to cathode through electrolyte. The currently available battery electrodes do not have enough capacity to intercalate Li ions in large amount and at the same time some of the intercalated Li is retained in the anode, thus reducing its capacity after few cycles. A gamut of research over the years has seen considerable development in battery technologies. Graphite anodes and lithium cobalt oxide ($LiCoO_2$) cathodes[1] are the most commonly used electrode materials in commercial Li-ion batteries. Graphite has been commonly used as an anode material for LIBs due to its high electronic (in-plane) conductivity as a result of delocalized π-bonds, and having appropriate structure for lithium ion intercalation and diffusion [1].

But, graphite has a restricted capacity (one lithium atom involving six carbon atoms to form LiC_6) and limited recharge rates [1, 2]. It is believed that carbon nanotubes (CNTs) can act as better anode for LIBs. Both, single and multiwalled CNTs have been examined by researchers for their usefulness as lithium storage material [1, 3-5]. CNTs have excellent properties; like low density, high mesoporosity [2] high aspect ratio of 100-1000, unique electrical and thermal as well as mechanical properties [6].

In LIBs, anode material is glued over copper foil which provides support to the anode. Although, copper act as a current collector and helps in charge transportation but it also increases the dead weight of the electrode which decreases the energy density of LIBs [5, 7]. LIBs with free standing anode shall be useful for light weight electronic devices. These electrodes have high specific energy density and capacity. Although previously free standing CNT bucky paper have been used by several researchers and their electrochemical properties have been reported [3, 4] but these suffer due to having poor mechanical properties. Thus, it is very difficult to handle these electrodes in the fabrication of batteries. Therefore, there is a need to develop a light weight free standing anode materials having good mechanical properties. The freestanding CNT bucky papers have poor mechanical properties. The mechanical properties can be improved by adding a suitable binding material (polymer). If a free standing electrode is used in place of cooper collector; it would have lighter weight. In order to improve the electrical conductivity of CNT loaded polymers, high loading of CNTs in the polymer matrix is required. But, it is very difficult to disperse high amount of CNTs (>5%) in any polymer matrix by conventional techniques. The reason behind this is the presence of strong Vander Waals forces between CNTs resulting in the formation of CNT bundles. For anode fabrication, it is necessary to incorporate large amount of CNTs into polymer matrix in order to achieve of high value of electrical conductivity. It has been

3

reported that CNTs have a tendency to agglomerate when more than 1 wt.% CNTs are loaded into polymer matrix[8]. Therefore, it is essential to look for a technique to incorporate higher amount of CNTs in the matrix without deteriorating its mechanical properties. Recently, several methods have been used to produce CNT/polymer composites having higher CNTs loading. In mechanical densification technique, vertically aligned CNTs were densified by capillary induced wetting with epoxy resin. [9]. Several other techniques have also been used, but most of them are limited by sample dimension. A filtration system was also used to incorporate epoxy resin into CNT bucky paper, however, complete impregnation of bucky paper with epoxy resin [10, 11] was very difficult. Feng et al, [12] reported a mixed curing-assisted layer-by-layer method to fabricate MWCNT/epoxy composite film with high CNT loading (15 to 36 wt. %). In this method, two type of curing agents were used, one was responsible for the partial initial curing at room temperature to avoid reagglomeration of the CNTs, and the other for complete curing of epoxy resin at higher temperature to make epoxy composite films having well-dispersed CNTs. In another study by Feng et al. [13], upto ~39.1 wt. % SWCNT loaded epoxy composites were produced using same layer by layer method and the mechanical properties of composite improved significantly. Macroscopic CNT composites having a high volume fraction (upto 27%) of millimeter long, well aligned CNTs were synthesized by Bradford et al. [14]. Shear pressing technique was used to process tall, vertically aligned CNT arrays into dense aligned CNT preforms, which were subsequently processed into composites. Ogasawara et al. [15] reported the fabrication of aligned MWCNT/epoxy composites by a hot-melt prepreg process. In another recent study by Singh et al. [8], upto 20 wt.% MWCNT were uniformly dispersed in epoxy resin and these were having improved mechanical properties (prepared using prepreg technique).

In the present study, a significant modification in the prepreg preparation technique using the phenolic resin in place of epoxy resin is reported. Phenolic resins have higher carbonization yield compared to epoxy resin and upto 46wt.% CNT loading can be achieved which is equivalent to 60 wt.% CNT loading in the final carbonized composite materials which would show excellent electrical conductivity. Thus, herein, we present a process for the fabrication of high loading CNT/phenolic composite paper which can be used as a free standing anode material and current collector in lithium ion battery. This electrode was tested for electrochemical performance. In addition to electrochemical properties, their electromagnetic interference shielding properties in the Ku-band (12.4-18 GHz) frequency was also studies. The electrical conductivity, open porosity, BET surface area, flexural strength, charge discharge capacity, impedance analysis, microstructure by SEM and HRTEM, spectroscopic analysis using Raman spectroscopy have also been studied.

Experimental

Materials

Phenolic resin obtained from 'IVP India Ltd.' was used as a carbonaceous resin for preparing composite paper. MWCNT were synthesized using toluene as a carbon source and ferrocene as a catalyst precursor in a home-made CVD set-up [16],. MWCNTs produced were having 26 nm average diameters and the average bundle length was ~350 µm [17]. These were 90 wt% pure with 10 wt% of Fe catalyst. These as-produced MWCNTs were graphitized in high temperature graphitization furnace (under inert atmosphere with a heating rate of 20°C/min upto 1500°C and subsequently 10°C/min upto 2600°C) and designated to G-CNT.

Fabrication of MWCNT-phenolic composites

5

0.5 gm MWCNT was dispersed in acetone. These dispersed MWCNTs were added in 30 gm phenolic resin (Novalac type) and mixed in acetone. Both suspension were then mixed together and homogenized using a high speed homogenizer (Miccra D-9, from ART Prozess and Labortechnik GmbH and co. KG) @ 30000 rpm for 5 min).   The dispersed CNTs in phenolic resin were filtered in a specially designed filtration unit to form a film of MWCNT impregnated resin and dried at 50°C for 15 min to form MWCNT-phenolic prepreg. The prepreg was compression moulded using hydraulic press by keeping them between two plates at 150°C for 2 h. The resultant composite paper was in the form of a uniform circular disc. The composite paper was carbonized in a programmable high temperature furnace under N$_2$ atmosphere up to 1000°C in steps (Room temp. to 600°C @ 50°C/h then 100°C/h upto 1000°C). These films were cut into desired shape for further testing. The schematic of complete procedure is shown in Fig. 1.
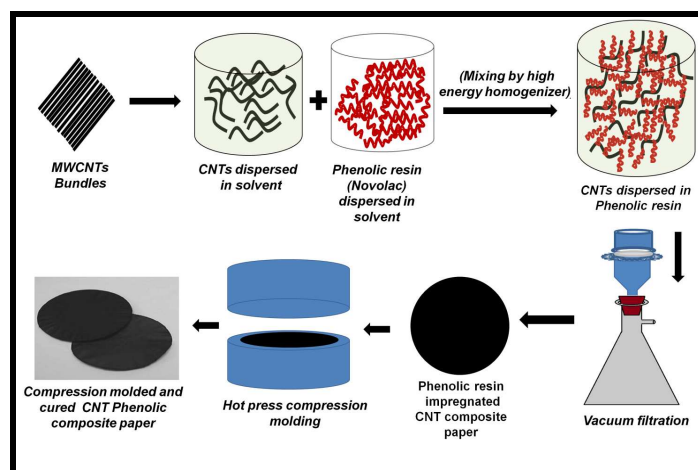
Fig. 1 Schematic of G-CNT/phenolic paper composite preparation

Characterization

The surface morphology of as-produced MWCNTs and G-CNT were analyzed using scanning electron microscopy (SEM) (Zeis Evo-50). HRTEM studies of as-produced and G-CNT were

carried out using Tecnai G20-stwin, 300 kV instrument. Raman studies of the as produced MWCNTs and G-CNT were carried out using Renishaw inVia Raman spectrometer, UK with an excitation source of 514.5 nm. The composite film samples were cut into rectangular shape for studying the mechanical properties. The flexural strength of the CNT/phenolic composite paper was measured using an INSTRON machine (model 4411). The length of the sample was 20 mm and span to depth ratio was kept 60:1 [18]. The cross head speed was kept fixed at 0.5 mm min^{-1}. For accuracy averages of three readings are taken. Specific surface area was calculated by BET method using autosorb iQ automated gas sorption analyzer from Quantacrome Instruments, USA (model no. ASIQM0000-4 and N_2 adsorption isotherm from Germany). The electrical conductivity of composite films (35 mm x 25 mm) was measured using dc four probe contact method by using a Keithley 224 programmable current source and Keithley 197 auto ranging digital microvoltmeter. The values reported in the text were averaged over five readings of voltage drops at different places on the samples. The free standing anode for testing in a half-cell was prepared by cutting an 18mm diameter circular specimen from the sample and drying in oven. The free standing electrode was then assembled into a test coin cell consisting of lithium foil as a counter electrode, a separator (polypropylene film) and organic electrolyte (1M $LiPF_6$ in 1:1 ratio of EC+DEC) in an argon-filled glove. The cell was allowed to age for 24 hours. The cells were charge–discharged at the C/10 rate and within the voltage range of 0.01–2.5V at room temperature, to determine the electrochemical characteristics.

Electromagnetic interference (EMI) shielding effectiveness (SE) were measured (by placing composite film in Ku-band (12.4-18 GHz) waveguides) using a vector network analyzer (VNA E8263B Agilent Technologies).

Results and Discussion

7

Morphological and structural studies

Fig. 2a and 2b shows the SEM micrographs of as produced MWCNT and G-CNT, respectively. The quality of the MWCNTs is improved after graphitization as shown by the SEM images (further confirmed by RAMAN studies and TEM).
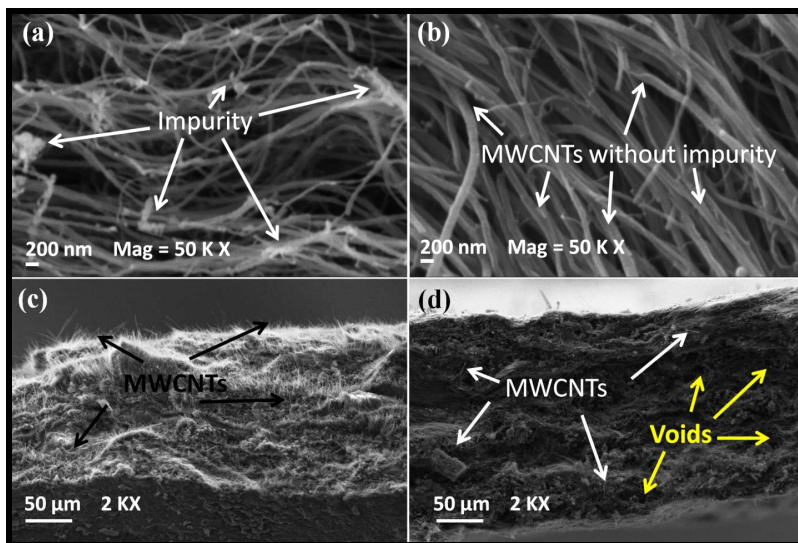
Fig. 2 SEM micrographs of (a) as-produced MWCNTs, (b) G-CNT, (c) and (d) fractured surface of cured non carbonised G-CNT/phenolic paper composite and carbonised G-CNT/phenolic paper composite, respectively.

Fig. 2c and 2d shows the fractured surface of cured non carbonised G-CNT/phenolic paper composite and carbonised G-CNT/phenolic paper composite, respectively. Cured non carbonised composite paper has pulled out MWCNTs which are suppressed during carbonisation. In the carbonised sample voids (shown by arrows in Fig. 2d) are created due to the removal of the volatile material during carbonisation, present in the resin.

TEM micrograph clearly shows that as-produced MWCNTs (fig. 3a) having some catalytic impurities on its surface which was removed after graphitization at 2600°C in induction furnace under inert atmosphere (Fig. 3b).
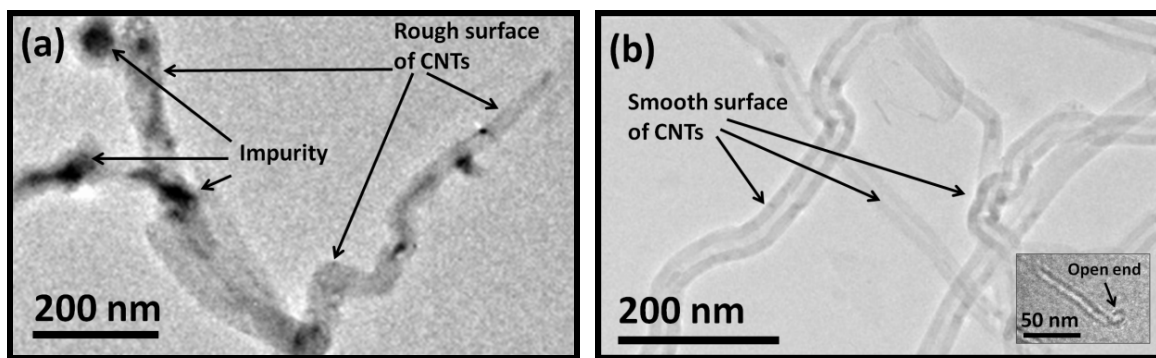
Fig. 3 TEM micrograph of (a) as-produce MWCNT and (b) G-CNT. The open end of G-CNT is shown in inset.

Inset of Fig. 3b shows that ends of MWCNTs are opened during graphitization which can contribute in better insertion of Li during cycling.

Raman spectroscopy is an extremely important technique generally used for the quick and non-destructive characterisation of all types of carbon. Raman spectrum of MWCNT consist of three important bands i.e. D band around 1350 cm^{-1}, G band around 1580 cm^{-1} and 2D (also called the G′ band) around 2700 cm^{-1}. G′ band is an overtone of the disorder induced D band positioned at ~1350 cm^{-1}. Both D and G′ bands arise due to an intervalley double resonance Raman process where the D band phonon scattering is a second order process intermediated by the defect, while the G′ band occurs due to scattering by two phonons and does need any defects for activation [19]. The D/G intensity ratio (I_D/I_G) represents most commonly for estimation of graphitisation index. This ratio monitors the amount of structural defects, or the extent of deviation of the crystalline arrangement from a perfect hexagonally organised planar carbon

9

network. The I_D/I_G ratio for as produced and G-CNT (fig 4) is 0.36 and 0.22, respectively. The significant reduction in the I_D/I_G ratio is due to increase in the crystallinity of the structure and reduction in the disordered structure. The G′/D intensity ratio ($I_{G'}/I_D$) is very sensitive to the overall crystalline quality of the graphitic network and enhances with increasing mean inter-defect distance and/or long-range ordering[20]. For the better quality high value of $I_{G'}/I_D$ (3.88 for GCNT and 2.81 for as produced CNTs) of MWCNTs is required where the organisation of C atoms becomes close to the ideal[20].
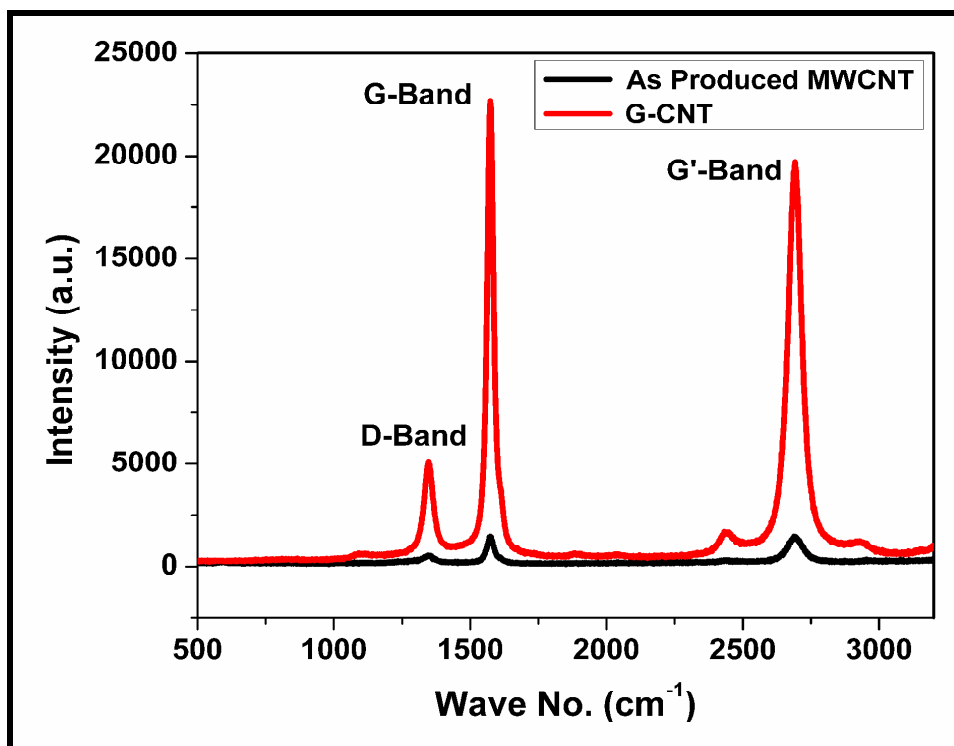

Fig. 4 Raman spectra of as-produced MWCNTs and G-CNTs

Table 1: Properties of non-carbonized and carbonized G-CNT/Phenolic composite paper

Properties	Non Carbonised	Carbonised
Thickness (mm)	0.16	0.14
Density (g/cc)	0.66	0.51
Conductivity (S/cm)	37	76
CNT (%)	45.9	60.6
Flexural Strength (MPa)	47	30
BET Surface area (m^2/g)	--	167

Table 1 summarizes the different properties of the composite paper. From the table, it can be seen that the sample is thin and the thickness decreases after carbonization. Composite samples have sufficient mechanical strength (flexural strength 47 MPa for non carbonized sample and 30 MPa for carbonized sample). During carbonization, some volatile substances evaporate resulting in decrease in the density of sample. It becomes slightly porous, and thickness decreases due to shrinkage, but the conductivity and CNT content get enhanced. Although, the overall CNTs content is same in both the cases but due to the removal of volatile substances the percentage of CNTs in carbonised sample increased which improves the conductivity from 37 Scm^{-1} to 76 Scm^{-1} after carbonization.

The specific surface area of carbonized composite sample was 167 m^2/g. Larger surface area provided more number of sites for Li ions insertion.

11

Electrochemical performance of anode

The charge discharge curve for sample cycled between 0.01 V to 2.5 V at C/10 rate is shown in Fig. 5.
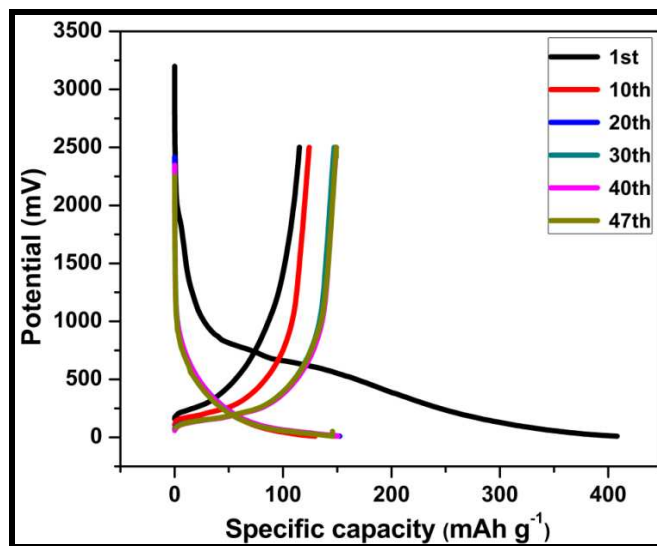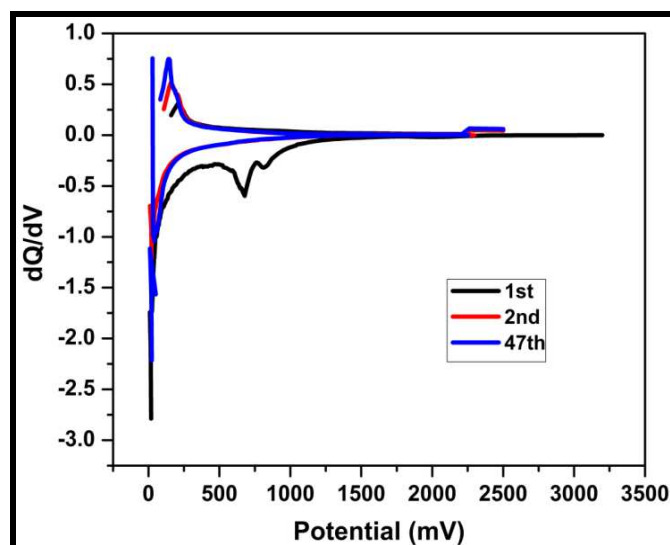

Fig. 5 Charge discharge curve for the carbonised G-CNT/phenolic composite paper (upto 47 cycles).

The 1st charge delivers 408 mAhg[-1] and the subsequent discharge capacity is 115 mAhg[-1]. The large irreversible capacity of 293 mAhg[-1] is due to (i) the initial decomposition of electrolyte at the electrode surface which forms solid electrolyte interface (SEI) and (ii) lithium being irretrievably trapped in the carbon matrix. The discharge capacity after 47 cycles is 147 mAhg[-1] which is in the range of general graphite based anode material. It is due to high surface area ~163 m^2/g of the free standing composite paper. The fabricated free standing anode has an advantage over the powder samples that it does not need current collector and mechanical support which adds to the dead weight of the cell/battery. In other words, these free standing highly conducting carbon based anode will have high energy density.
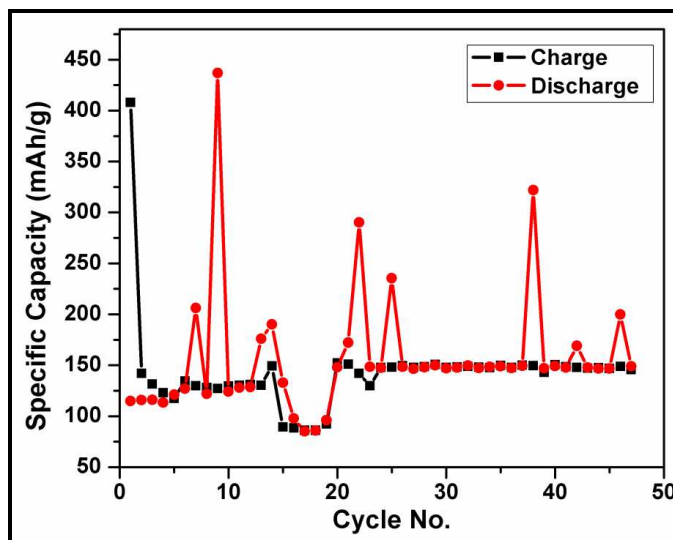
Fig. 6 Specific capacity of carbonised G-CNT/phenolic composite paper

Fig. 6 shows the charge-discharge studies of the sample. The capacity increases and becomes stable after 20 cycles. The increase in capacity may be due to the de-intercalation of Li ions trapped during the previous cycles. There is a capacity drop between cycles no 15 to 20. It may be possible due to the some of Li inserted into the anode has not come out in these cycles.

Fig. 7 Differential capacity curve for the 1st, 2nd and 47th cycle

13

Fig. 7 exhibits differential capacity curve for the charge-discharge cycle of the cell. The charge discharge curve shows that the peak starts around 0 to 0.5 V. Since this plot is considered equivalent to the cyclic voltammetry, the insertion and extraction potential is derived from the peak positions. On charging, the peak potential shifts from 227 to 132 mV for 1st to 47th cycles, respectively. It may be due to the SEI formed which is very stable. In general, the lower insertion potential of anode materials, the higher the total voltage of cell, therefore the shift to lower potential is very significant for the lithium ion battery performance.
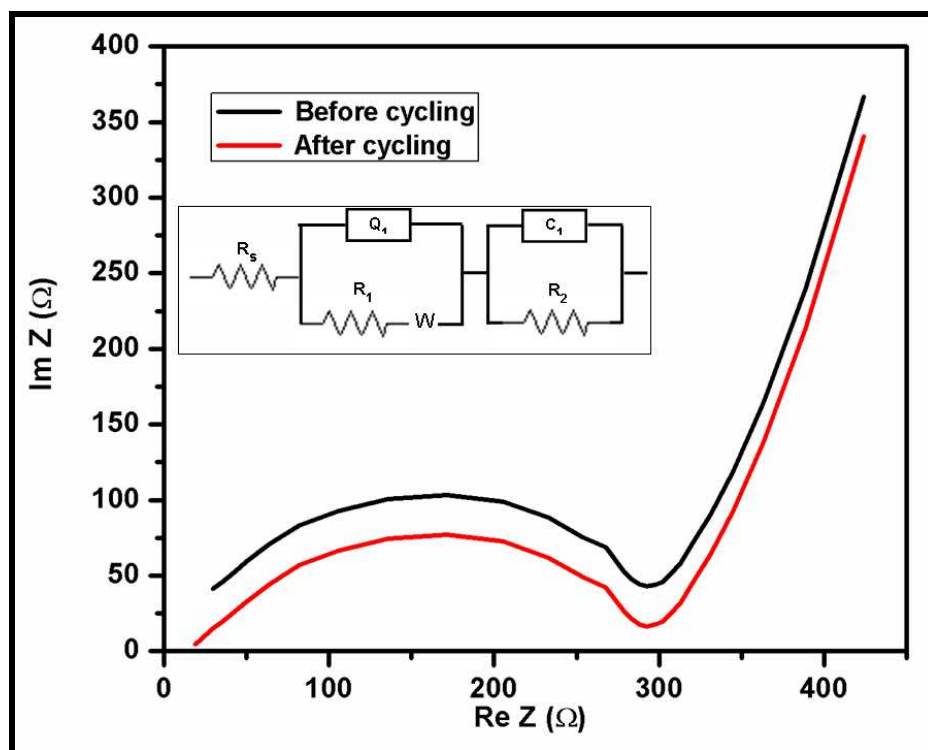
Fig. 8 Nyquist plot of the carbonised G-CNT/phenolic composite paper before and after cycling and inset shows corresponding equivalent circuit

Electrochemical impedance studies were also carried out on the samples for further understanding the cell performance. The electrolyte resistance (R_S) of sample cell increases from

10 to 15 ohm indicating a slight decrease in the ion concentration and/ or ion mobility in the electrolyte solution.

The semicircle obtained in the Nyquist plots (Fig. 8) correspond to properties related to Li ion migration through the solid/electrolyte interface (SEI) layer. The charge transfer resistance (R_{CT}) of the sample cell was calculated by extrapolating the semicircle and the estimated value was 310 ohm. After cycling the charge transfer resistance decreases to 295 ohm.

The impedance plot is fitted and the equivalent circuit is arrived as in the inset figure 8 and the values are tabulated in Table 2. It explains that for the both electrochemical impedance spectroscopy (EIS) data, equivalent circuit is same. The capacitance Q_1 is in the order of μF which shows the lower double layer capacitance at the electrode interface. The R_1 is 277.1 and 275 Ω of the before and after cycling respectively shows that there is no significant change during the cycling process. C_1 is the bulk capacitance of the material and R_2 is the leakage resistance.

The lithium diffusion coefficient is calculated from the lower frequency region by using the formula $D = R^2 \times T^2 / 2A^2 n^4 F^4 C^2 \sigma^2$ where the σ is calculated from the equation $Z_{re} = R_D + R_L + \sigma\omega^{-1/2}$ by plotting $\omega^{-1/2}$ Vs Z_{re}. Consequently the diffusion coefficient values of both the EIS spectra shows in the order of 10^{-17} which is ideal for the lithium diffusion at the electrode interface.

Table 2: EIS parameters of carbonised G-CNT/phenolic composite paper before and after cycling

	Rs(ohm)	$Q_1(\mu F)$	n	$R_1(ohm)$	W	$C_1(mF)$	$R_2(ohm)$	Diffusion coefficient (cm^2s^{-1})
Before	7.6	1.295	0.796	277.1	210	1.723	5078	1.36449×10^{-17}
After	18.2	19.46	0.629	275	93.98	8.361	4300	1.27455×10^{-17}

As can be seen from table 1, G-CNT/ phenolic composite paper prepared by carbonization at 1000°C retains significant properties of CNT (such as dc electrical conductivity, and mechanical strength). Most importantly, these samples show optimum value of conductivity which is desired for exhibiting good microwave shielding response. Hence, one would expect that these materials could be potentially used in several applications; such as; as the anode for Li-ion battery, as anode for fuel cell [21-23] and in EMI shielding devices. In view of the fact that our composite paper is conducting and have good mechanical strength, we have studied its EMI shielding properties.

Electromagnetic interference (EMI) shielding

For EMI shielding measurements, composite sample was inserted into the sample holder of size 15.8×7.9 mm^2. The SE was measured by calculating scattering parameters following the procedures reported earlier[17, 24-31].

16
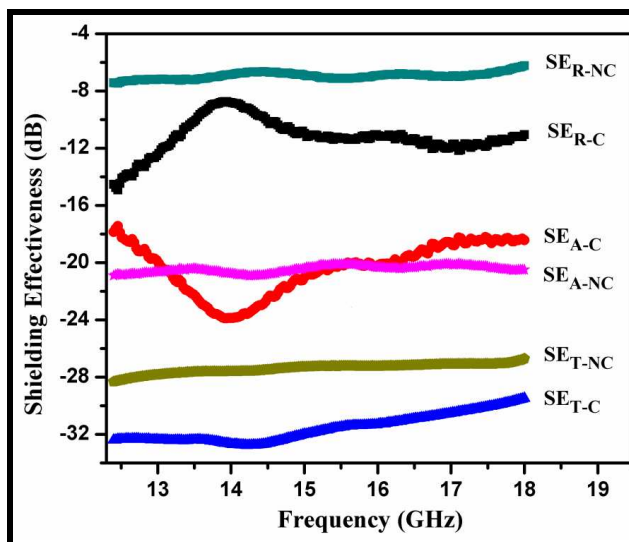
Fig. 9 EMI SE$_T$, SE$_A$ and SE$_R$ of G-CNT/phenolic composite paper carbonized and non - carbonized as a function of frequency

Fig. 9 shows variation of shielding effectiveness (SE) in 12.4−18 GHz frequency range. The value of SE due to absorption (SE$_{A-NC}$) and reflection (SE$_{R-NC}$) by non-carbonized G-CNT/Phenolic composite paper are 20.9 dB and 9 dB, respectively. Thus, the total SE$_{T-NC}$ achieved by the non-carbonized G-CNT/Phenolic composite paper is 29.9 dB. While for carbonized G-CNT/phenolic composite paper, SE$_{A-C}$ and SE$_{R-C}$ values were 17.9 dB and 14.5 dB, respectively. Thus, the total SE$_{T-C}$ by carbonized composite paper is 32.4 dB which is significantly higher than by the non-carbonized paper. It is due to significant enhancement in the electrical conductivity of carbonized sample over the non carbonized sample. A SE value of around 20 dB is required for commercial EMI shielding applications [32]. Hence, our carbonized G-CNT/phenolic composite paper can be used for commercial EMI shielding applications.

Results suggest that SE$_T$ is mainly due to absorption, while the contribution from reflection (SE$_R$) is lesser. The primary mechanism of EMI shielding is reflection of the

17

electromagnetic radiation; which is a consequence of interaction of EMI radiation with the free

electrons on the surface of the conducting shield [33].

The excellent shielding performance of carbonized composite paper is mainly attributed

to two factors: impedance matching and EM wave attenuation. The presence of conducting

MWCNT in the insulating phenolic resin matrix results in the formation of large number of

interfaces and a heterogeneous system due to accumulation of space-charge at the interface

which contributes toward higher microwave shielding by the composites. Due to difference in

the conductivity of MWCNT and resin, some charge carriers present in MWCNT get trapped,

resulting in development of space-charge on the surface of the resin matrix. The contribution

from ionic conduction toward total loss becomes exceptionally higher at frequency. With

increase in frequency, the interfacial polarization decreases resulting in decrease in polarizability

and loss factor. All these phenomena play crucial roles in the enhancement of microwave

shielding. It may be proposed that the presence of MWCNT in carbonized paper leads to

reduction of skin depth and increase in conductivity along with improvement in input impedance.

This not only enhances the amount of electromagnetic radiation penetrating inside the shield but

also increases the effective absorption capability. The presence of MWCNT in phenolic resin

results in (i) formation of large number of interfaces, and (ii) a heterogeneous system due to the

presence of space charge at the interface, which allows impedance matching for better

microwave shielding.

Conclusion

Strong, light weight and free standing MWCNT/phenolic composite paper was fabricated using a

simple and novel dispersion technique. MWCNTs produced in-house by CVD were graphitized

to improve its quality. The paper has very good electrical conductivity (76 Scm^{-1}) and bending strength (30 MPa) to be used as anode in LIBs without the need of copper as current collector, thus reducing the weight and increasing the energy density. It exhibits a stable reversible specific capacity for more that 45 cycles of operation. The thin paper (thickness ~ 140 μm) shows efficient electromagnetic shielding effectiveness of 32.4 dB which surpasses the value needed for commercial applications.

Acknowledgements

1. N. A. Kaskhedikar and J. Maier, *Advanced Materials*, 2009, **21**, 2664-2680.
2. W. Lu, A. Goering, L. Qu and L. Dai, *Physical Chemistry Chemical Physics*, 2012, **14**, 12099-12104.
3. C. Kang, I. Lahiri, R. Baskaran, W.-G. Kim, Y.-K. Sun and W. Choi, *Journal of Power Sources*, 2012, **219**, 364-370.
4. D. T. Welna, L. Qu, B. E. Taylor, L. Dai and M. F. Durstock, *Journal of Power Sources*, 2011, **196**, 1455-1460.
5. B. J. Landi, M. J. Ganter, C. D. Cress, R. A. DiLeo and R. P. Raffaelle, *Energy & Environmental Science*, 2009, **2**, 638-654.
6. V. Choudhary, B. Singh and R. Mathur, *Carbon Nanotubes and Their Composites, Syntheses and Applications of Carbon Nanotubes and Their Composites, ed. Dr S. Suzuki, ISBN*, 2013, 978-953.
7. B. J. Landi, R. A. Dileo, C. M. Schauerman, C. D. Cress, M. J. Ganter and R. P. Raffaelle, *Journal of Nanoscience and Nanotechnology*, 2009, **9**, 3406-3410.

8.   B. P. Singh, Prasanta, V. Choudhary, P. Saini, S. Pande, V. N. Singh and R. B. Mathur, *Journal of Nanoparticle Research*, 2013, **15**, 1-12.

9.   B. L. Wardle, D. S. Saito, E. J. García, A. J. Hart, R. G. de Villoria and E. A. Verploegen, *Advanced Materials*, 2008, **20**, 2707-2714.

10.   J. Gou, *Polymer International*, 2006, **55**, 1283-1288.

11.   Z. Wang, Z. Liang, B. Wang, C. Zhang and L. Kramer, *Composites Part A: Applied Science and Manufacturing*, 2004, **35**, 1225-1232.

12.   Q.-P. Feng, J.-P. Yang, S.-Y. Fu and Y.-W. Mai, *Carbon*, 2010, **48**, 2057-2062.

13.   Q.-P. Feng, X.-J. Shen, J.-P. Yang, S.-Y. Fu, Y.-W. Mai and K. Friedrich, *Polymer*, 2011, **52**, 6037-6045.

14.   P. D. Bradford, X. Wang, H. Zhao, J.-P. Maria, Q. Jia and Y. T. Zhu, *Composites Science and Technology*, 2010, **70**, 1980-1985.

15.   T. Ogasawara, S.-Y. Moon, Y. Inoue and Y. Shimamura, *Composites Science and Technology*, 2011, **71**, 1826-1833.

16.   R. B. Mathur, S. Chatterjee and B. P. Singh, *Composites Science and Technology*, 2008, **68**, 1608-1615.

17.   B. P. Singh, K. Saini, V. Choudhary, S. Teotia, S. Pande, P. Saini and R. B. Mathur, *J Nanopart Res*, 2014, **16**, 2161.

18.   R. B. Mathur, P. H. Maheshwari, T. L. Dhami, R. K. Sharma and C. P. Sharma, *Journal of Power Sources*, 2006, **161**, 790-798.

19.   R. Rao, R. Podila, R. Tsuchikawa, J. Katoch, D. Tishler, A. M. Rao and M. Ishigami, *ACS Nano*, 2011, **5**, 1594-1599.

20.   S. Santangelo, G. Messina, G. Faggio, M. Lanza and C. Milone, *Journal of Raman Spectroscopy*, 2011, **42**, 593-602.

21.   Z. Q. Tian, S. P. Jiang, Y. M. Liang and P. K. Shen, *The Journal of Physical Chemistry B*, 2006, **110**, 5343-5350.

22.   M. M. Shaijumon, S. Ramaprabhu and N. Rajalakshmi, *Applied Physics Letters*, 2006, **88**, 253105-253105-253103.

23.   A. P. Singh, B. K. Gupta, M. Mishra, Govind, A. Chandra, R. B. Mathur and S. K. Dhawan, *Carbon*, 2013, **56**, 86-96.

24.   P. Saini, V. Choudhary, B. Singh, R. Mathur and S. Dhawan, *Materials Chemistry and Physics*, 2009, **113**, 919-926.

25.   T. K. Gupta, B. P. Singh, V. N. Singh, S. Teotia, A. P. Singh, I. Elizabeth, S. R. Dhakate, S. K. Dhawan and R. B. Mathur, *Journal of Materials Chemistry A*, 2014, **2**, 4256-4263.

26.   T. K. Gupta, B. P. Singh, R. B. Mathur and S. R. Dhakate, *Nanoscale*, 2014, **6**, 842-851.

27.   A. P. Singh, M. Mishra, P. Sambyal, B. K. Gupta, B. P. Singh, A. Chandra and S. K. Dhawan, *Journal of Materials Chemistry A*, 2014.

28.   T. K. Gupta, B. P. Singh, S. R. Dhakate, V. N. Singh and R. B. Mathur, *J. Mater. Chem. A*, 2013, 9138-9149.

29.   T. K. Gupta, B. P. Singh, S. Teotia, V. Katyal, S. R. Dhakate and R. B. Mathur, *Journal of Polymer Research*, 2013, **20**, 1-7.

30.   K. Singh, A. Ohlan, V. H. Pham, R. Balasubramaniyan, S. Varshney, J. Jang, S. H. Hur, W. M. Choi, M. Kumar and S. Dhawan, *Nanoscale*, 2013, **5**, 2411-2420.

31.   B. P. Singh, V. Choudhary, P. Saini and R. B. Mathur, *AIP Adv*, 2012, **2**, 022151.

32.   N. Li, Y. Huang, F. Du, X. He, X. Lin, H. Gao, Y. Ma, F. Li, Y. Chen and P. C. Eklund, *Nano Letter*, 2006, **6**, 1141-1145.

33.   D. D. L. Chung, *Carbon*, 2001, **39**, 279-285.